J Mater Sci (2007) 42:5375–5380
DOI 10.1007/s10853-006-0892-z

Formation of bulk Cu_6Sn_5 intermetallic compounds in Sn–Cu lead-free solders during solidification

J. Shen · Y. C. Liu · H. X. Gao

Received: 5 February 2006 / Accepted: 25 August 2006 / Published online: 22 March 2007
© Springer Science+Business Media, LLC 2007

Abstract The influence of cooling rate and Cu content on the microstructures of the solidified Sn–Cu alloys was investigated in terms of microstructural observation, thermal analysis and theoretical calculation. It was found that bulk Cu_6Sn_5 intermetalic compounds (IMCs) formed only in the Sn–1.0Cu alloy with lower cooling rate. At higher cooling rate, the actual eutectic point of Sn–Cu solder alloy shifts to the direction of higher Cu concentration. Thus the eutectic and hypereutectic alloys experience a metastable pseudoeutectic solidification route instead. The volume fraction of the bulk Cu_6Sn_5 IMCs formed in the Sn–1.0Cu alloy, measured by thermal analysis, is larger than that predicted by the equilibrium phase diagram. This could be attributed to eutectic Cu_6Sn_5 phases, which cling to the primary Cu_6Sn_5 crystal during the eutectic reaction due to their matching crystalline orientation relationship.

Introduction

Tin-lead solder has been used since 2000 years ago and it is still widely used in the assembly of modern electronic circuits. However, the increasing considerations on the environmental protection and health hazards of Tin-lead solder, which was used in electronic packaging, have prompted the development of alternative lead-free solders in electronic industry [1–3]. Among the various lead-free solders, Sn–Cu alloy has received more attention due to its competitive lower price, which makes it potentially attractive in actual applications for consumer products. Although the inferior wettability and Tin Whiskers of Sn–Cu alloy might be the issues for its application, it was still recognized as one of the cheapest choice in lead-free solders for replacing conventional Sn–Pb eutectic alloy [4, 5].

In addition, the interfacial reactions between lead-free solders and substrate may affect the mechanical performance of solder joint. During the soldering, the solder alloy melts and then reacts with the substrate to form IMCs at the joint interface. With the formation of a thin IMC layer a better metallurgical bond can be achieved. However, excessive IMC growth may have a deleterious effect. Hence, many researchers have focused on the study of interfacial reaction between Sn–Cu alloy and substrate as well as the growth kinetics of IMCs [6–12].

The solidification process of Sn–Cu solder alloy also has effects on the mechanical performance of solder joint. The brittle Cu_6Sn_5 IMCs formed in this alloy during solidification could deteriorate the joint reliability. However, the formation mechanism of Cu_6Sn_5 IMCs in Sn–Cu solder during solidification has not been fully understood, especially for the large Cu_6Sn_5 IMCs.

In this study, the influence of cooling rate and Cu content on the microstructures of the solidified Sn–Cu alloys was investigated in terms of microstructural observation, thermal analysis and theoretical calculation. In addition, the formation and growth mechanisms of large Cu_6Sn_5 IMCs in lead-free Sn–Cu solders were also discussed in details.

J. Shen (✉)
College of Mechanical Engineering, Chongqing University, Chazheng street 174, Chongqing 400044, P.R. China
e-mail: shenjun2626@163.com

Y. C. Liu · H. X. Gao
College of Materials Science & Engineering, Tianjin University, Weijin road 92, Tianjin 300072, P.R. China

Experimental procedure

Sn–0.7Cu eutectic alloy and Sn–1.0Cu hypereutectic alloy were prepared from ingots of pure Sn and Cu (with a purity of 99.99%). The melting process was carried out in a vacuum arc furnace under the protection of high purity argon atmosphere to produce buttonlike specimens with a diameter of approximately 3.5 cm. In order to obtain a homogeneous composition, all ingots were remelted for four times.

The Sn–Cu master alloy was then cut into small specimens with a dimension of $\phi 5 \times 2$ mm. Those specimens were then heated up and cooled down to room temperature with different cooling rates of 10 K min^{-1} (slowly cooled) and about 6×10^3 K min^{-1} (rapidly-cooled) respectively. In this study, the cooling rates were controlled by changing the cooling media: the slow cooling rate was achieved in Differential Thermal Analysis (DTA) apparatus, and the rapid cooling rate was obtained by casting it into a water-cooled copper mold.

The Sn–Cu specimens were polished and etched with a solution of 5 vol. % HNO_3 + 95 vol. % C_2H_5OH. Optical Microscopy (OLYMPUS BX51M) was adopted for the observation of microstructure. X-ray diffraction (Rigaku D/max 2500v/pc) was adopted for the determination of phase structure in the slowly cooled Sn–1.0Cu alloy. Additionally, energy diffraction spectrometer (OXFORD ISIS300) was used to determine the phase composition of the white plate structure in the slowly cooled Sn–1.0Cu alloy.

A Netzsch DSC 404C apparatus was adopted for DTA measurements. The isochronal measurement DTA signals were calibrated and corrected by the melting point of pure Sn and heat capacity of sapphire according to the method described in Ref. [13]. This common method of heat capacity calibration in non-isothermal DTA is to calculate the value of the apparent heat capacity of a sample ($C_{p,s}^{\mathrm{app}}$) assuming that the measure temperature difference is proportional to the heat capacity of the specimen:

$$C_{p,s}^{\mathrm{app}} = C_{p,\mathrm{cal}} \frac{\Delta T_{t,s}}{\Delta T_{t,\mathrm{cal}}} \tag{1}$$

where $C_{p,\mathrm{cal}}$ is the heat capacity of the calibration material (which equals the product of the number of moles of the calibration material and the literature value for the molar heat capacity of the calibration material), $\Delta T_{t,s}$ and $\Delta T_{t,\mathrm{cal}}$ are the measurement signals from the DTA measurements on the calibration material and on the sample, respectively. Thus, determined value for the heat capacity is an apparent heat capacity because the influence of smearing over time is neglected.

DTA measurement was done under the protection of high-purity argon to avoid any unexpected oxidation. The applied thermal treatment procedure in the calorimetric experiment was as follows: the Sn–1.0Cu specimen was firstly heated from room temperature up to 543 K with a constant heating rate of 10 K min^{-1} and kept at this temperature for 10 min. It was then cooled down to room temperature with a rate of 10 K min^{-1}.

Results and discussion

Formation of bulk Cu_6Sn_5 IMCs

According to the Sn–Cu equilibrium phase diagram illustrated in Fig. 1, Sn–0.7Cu and Sn–1.0Cu alloys experience equilibrium eutectic and hypereutectic reaction, respectively. Figure 2 illustrates the corresponding solidification routes of Sn–Cu alloys under the slow and rapid cooling conditions. Under equilibrium solidification condition (eutectic reaction point is *a*), Sn–0.7Cu and Sn–1.0Cu alloys would experience eutectic and hypereutectic reactions, respectively. The corresponding equilibrium solidification points were *a* (Sn–0.7Cu alloy) and *c* (Sn–1.0Cu alloy) and the equilibrium solidification paths can be described as:

Eutectic reaction: $L \rightarrow Cu_6Sn_5 + \beta$ - Sn

Hypereutectic solidification path: $L \rightarrow L$ + primary Cu_6Sn_5 crystal and $L \rightarrow Cu_6Sn_5 + \beta$ - Sn

Figure 3a and b illustrate the typical microstructures of the slowly cooled Sn–0.7Cu and Sn–1.0Cu samples, which nearly follow the corresponding equilibrium solidification path as presented above. According to the X-ray diffraction spectrum (see Fig. 4) of the slowly cooled Sn–1.0Cu alloy and EDS analysis results (see Table 1) of white plate phase in it, it is obvious that these slowly cooled alloys exhibit

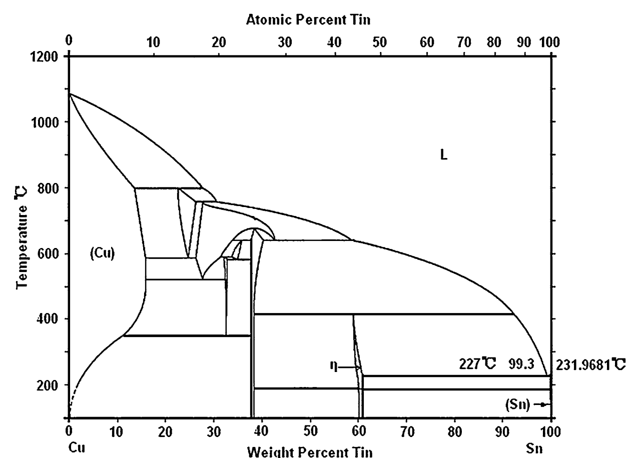

Fig. 1 Binary phase diagram of Sn–Cu system

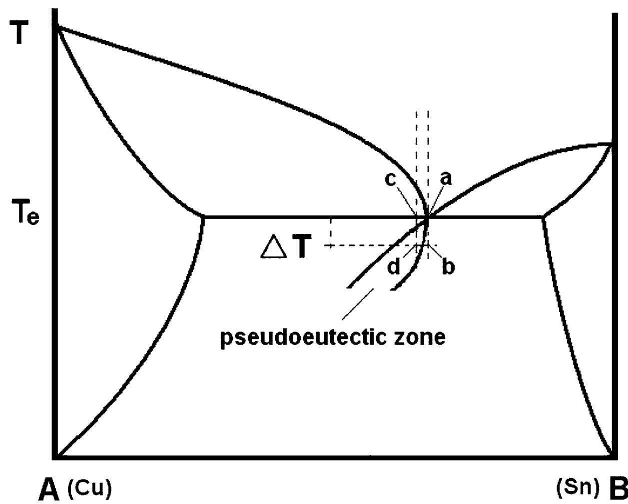

Fig. 2 Schematical diagram of the Sn–Cu alloys solidified with/without the kinetic undercooling

Table 1 EDS analysis results of white plate-like structure in slowly cooled Sn–1.0Cu alloy

Composition, at. %		Phase identification
Sn	Cu	
46.35 ± 0.28	53.65 ± 0.18	Cu_6Sn_5

eutectic (full gray eutectic colonies) and hypereutectic (white bulk Cu_6Sn_5 IMCs and gray eutectic colonies) structures.

For rapid cooling condition, the achieved degree of kinetic undercooling, ΔT, leads to the metastable eutectic concentration shifting to higher Cu concentration. Although the β-Sn phase requires an undercooling more than that of the Cu_6Sn_5 during solidification [14], the obtained kinetic undercooling ΔT is enough for the formation of the β-Sn phase. Therefore, the corresponding non-equilibrium solidification points were *b* (Sn–0.7Cu alloy) and *d* (Sn–1.0Cu alloy). Furthermore, the Sn–0.7Cu eutectic alloy exhibits hypoeutectic microstructure which consists of a mixture of primary β-Sn dendrites and gray eutectic colonies (as seen in Fig. 3c). The Sn–1.0Cu hypereutectic alloy exhibits a large number of regular eutectic lamellar structures, including alternative white (β-Sn phase) and dark (Cu_6Sn_5 phase) lamellas along the growth direction (as seen in Fig. 3d).

Microstructural observation indicates that the bulk plate-like Cu_6Sn_5 IMCs only formed in the slowly cooled Sn–1.0Cu alloy. It seems that this bulk Cu_6Sn_5 IMCs is same as the primary Cu_6Sn_5 crystal formed in the Sn–1.0Cu alloy during solidification. Following the equilibrium solidification process, the volume fraction of primary Cu_6Sn_5 crystal formed in Sn–1.0Cu alloy could be determined by ''*lever rule*'' according to the phase diagram [15]. During the hypereutectic solidification processes, the Sn–1.0Cu liquid alloy matches with the eutectic composition after the proeutectic reaction (i.e., the end of primary Cu_6Sn_5 crystal formation). The concentration for equilibrium eutectic reaction can be formulated as:

$$\frac{C_{\mathrm{Cu}} - C_p}{C_{\mathrm{Sn}} - {}^5\!/_6 C_p} = {}^{1.3}\!/_{98.7} \tag{2}$$

where C_{Cu} is the Cu concentration and C_{Sn} is the Sn concentration in Sn–1.0Cu alloy. Here, C_p is the Cu concentration in primary Cu_6Sn_5 crystal in the solidified Sn–1.0Cu

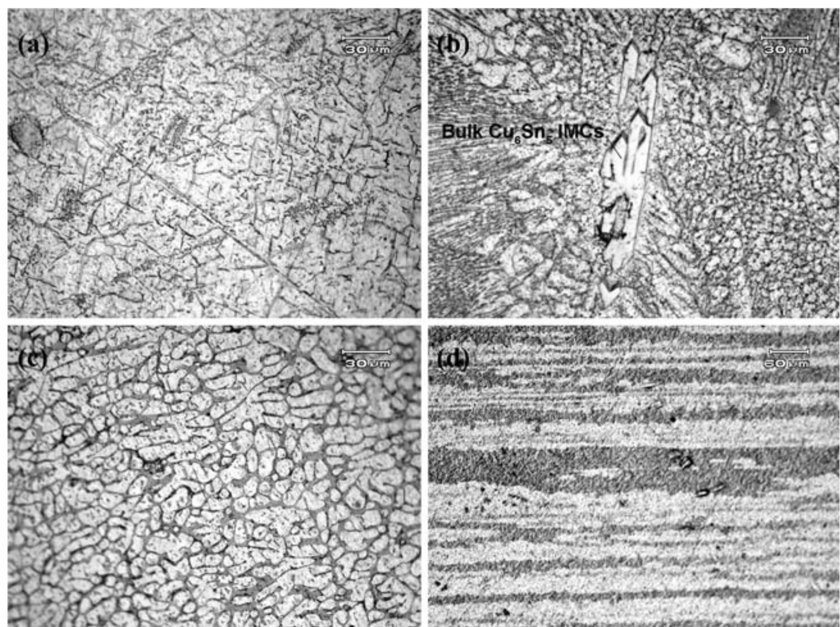

Fig. 3 Optical microstructures of Sn–Cu alloys, (**a**) slowly cooled Sn–0.7Cu alloy, (**b**) slowly cooled Sn–1.0Cu alloy, (**c**) rapidly-cooled Sn–0.7Cu alloy and (**d**) rapidly-cooled Sn–1.0Cu alloy

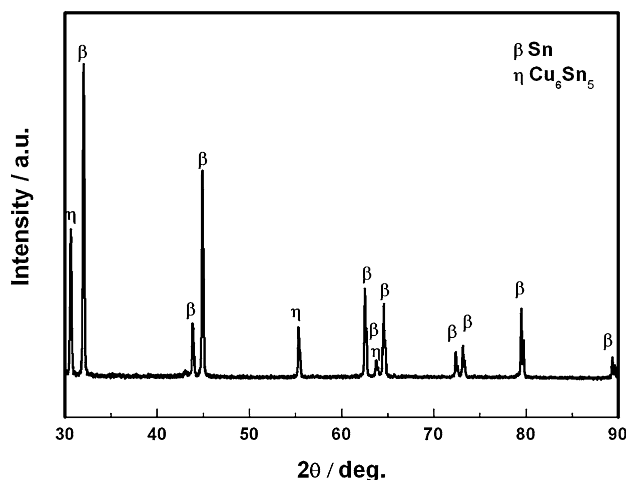

Fig. 4 X-Ray diffraction spectra of the slowly cooled Sn–1.0Cu alloy

alloy. Sn concentration in the primary Cu_6Sn_5 crystal in solidified Sn–1.0Cu alloy is $^5/_6$ C_p. Noted in Eq. (2), that the atomic percentage has to be adopted. Finally, C_p arrives at about 0.51 mol% by adopting Eq. (2). Since the actual solidification process (under slow cooling) is slightly far from the equilibrium state, the volume fraction of primary Cu_6Sn_5 crystal in the explored slowly cooled Sn–1.0Cu alloy must be smaller than 0.51.

Growth of bulk Cu_6Sn_5 IMCs

The volume fraction of the bulk Cu_6Sn_5 IMCs was determined by measuring the apparent heat capacities curve of hypereutectic Sn–1.0Cu alloy. Figure 5 illustrates the measured apparent heat capacities of Sn–1.0Cu alloy solidified with a cooling rate of 10 K min^{-1}. The peak

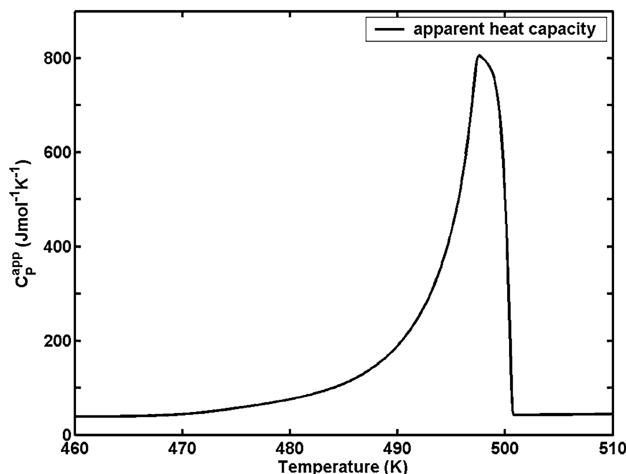

Fig. 5 Apparent heat capacity of Sn–1.0Cu alloy solidified with cooling rates of 10 K min^{-1}

corresponds to the solidification reaction of Sn–1.0Cu alloy.

A general procedure for the determination of transformed bulk Cu_6Sn_5 fraction from the solidified solder in the recorded apparent heat capacity curve was adopted [16]. The liquid fraction, f_l, and the enthalpy difference between the liquid and solid ΔH_{st}, have been determined as a function of temperature in the measured curves of apparent heat capacity. The apparent heat capacity, $C_{p,m}$, includes the heat of transformation and the change in the heat capacity of liquid, $C_{p,l}$, and of solid, $C_{p,s}$, induced by temperature change:

$$C_{p,m}(T) = f_l C_{p,l}(T) + f_s C_{p,s}(T) + \frac{df_s}{dT} \Delta H_{sl}(T) \quad (3)$$

where the solid fraction, f_s, equals $1\text{–}f_l$. The first two terms at the right-hand side of the above equation state that the heat capacity of both liquid and solid phases can be given as the weighted (according to the amounts of the individual phases) average of the heat capacities of the individual phases. The last term at the right-hand side represents the (reaction) enthalpy releasing during solidification. The values of $C_{p,l}$ and $C_{p,s}$ can be determined by extrapolation from the measured $C_{p,m}$ outside of the temperature range where the solidification takes place.

The temperature dependent enthalpy difference is caused by the difference between the temperature dependent heat capacities of the separate phases:

$$\Delta H_{sl}(T) = H_0 + \int_{T_1}^{T_2} (C_{p,s}(T) - C_{p,l}(T)) dT \quad (4)$$

where H_0 is the value of ΔH_{sl} at the starting temperature of transformation T_1, which is to be determined according to the following procedure. The starting point of the transformation, where f_l equals 1, is estimated by comparing the measured $C_{p,s}$ curve with the extrapolated curve for $C_{p,l}$, T_2 is the temperature where the transformation has just been completed (i.e. $f_s = 1$). By prescribing H_0, ΔH_{sl} can be calculated as a function of temperature from T_1 to T_2. These values of ΔH_{sl} are used as inputs to evaluate f_l from the measured $C_{p,s}$. Then the value of H_0 is adjusted in order to satisfy the requirement that the fraction f_s equals 1 at $T = T_2$.

Using the above method, the fraction of solid phase and the determined transformation rate were obtained from the measured apparent heat capacities (Fig. 5). The transformation rate of the solid phase in the investigated Sn–1.0Cu alloy, with applied cooling rate of 10 K min^{-1}, was calculated and presented as a function of temperature in Fig. 6. Two inflection points could be recognized in the obtained curves of the transformation rate. After comparing

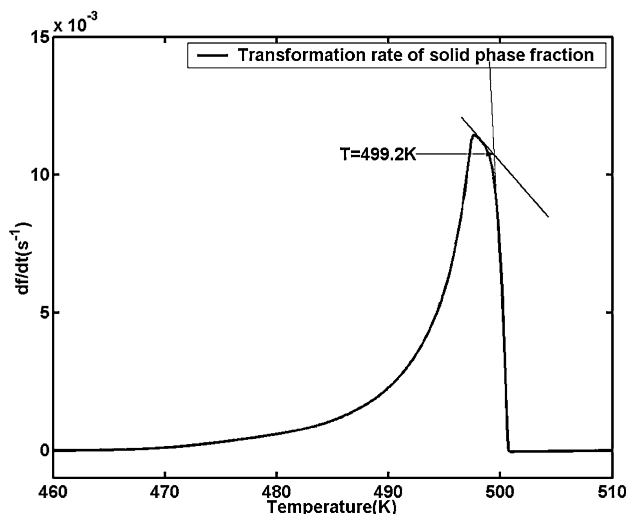

Fig. 6 The relationship between the solid fraction transformation rate and temperature as determined from DSC measurement of Sn–1.0Cu alloy at the cooling rates of 10 K min^{-1}

with the schematical diagram of Fig. 2, it is found that the low inflection point is mainly from the formation of bulk Cu_6Sn_5 IMCs (corresponding to the white bulk plate-like structure, in Fig. 3b), and the high inflection point is from the eutectic reaction (corresponding to the gray area in Fig. 3b). Hence, the first inflection point is likely the ending point of bulk Cu_6Sn_5 IMCs formation.

Figure 7 shows the relationship between the solid fraction and temperature as determined from DSC measurement of Sn–1.0Cu alloy. According to Fig. 6, the ending temperature point of bulk Cu_6Sn_5 IMCs formation was achieved, and it was used to determine the volume fraction

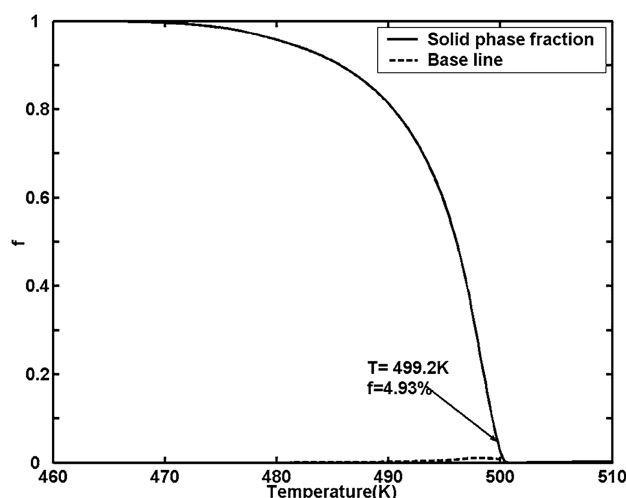

Fig. 7 The relationship between the solid fraction and temperature as determined from DSC measurement of Sn–1.0Cu alloy at the cooling rates of 10 K min^{-1}

of the bulk Cu_6Sn_5 IMCs (Fig. 7). The volume fraction (4.93) of bulk Cu_6Sn_5 IMCs, determined from the measured apparent heat capacity, is larger than the volume fraction (0.51) of primary Cu_6Sn_5 crystal in the solidified Sn–1.0Cu alloy. Hence, the bulk Cu_6Sn_5 IMCs formed in the Sn–1.0Cu alloy is not totally from the primary Cu_6Sn_5 crystals predicted by the equilibrium phase diagram.

The inherent mechanism for the formation of excessive bulk Cu_6Sn_5 IMCs in slowly cooled Sn–1.0Cu alloy could be explained by the schematical diagram shown in Fig. 8. The two phases involved possess different growth velocities, and the leading phase is Cu_6Sn_5 during the eutectic reaction of Sn–Cu alloy [17]. Hence, if primary Cu_6Sn_5 crystals formed before the onset of eutectic reaction (such as slowly cooled Sn–1.0Cu alloy), the leading Cu_6Sn_5 phase could nucleate adjacent to the primary Cu_6Sn_5 crystal for their matching crystalline orientation relationships, which would result in the formation of bulk Cu_6Sn_5 IMCs. Thus the solidified volume fraction of bulk Cu_6Sn_5 IMCs becomes larger than the amount of primary Cu_6Sn_5 crystals predicted by the equilibrium phase diagram.

When β-Sn phase acts as the primary phase (such as rapidly-cooled Sn–0.7Cu alloy), it requires more driving force (high undercooling) for the Cu_6Sn_5 phase to separate through an eutectic reaction and cling around the primary β-Sn crystal. This is caused by the mismatched crystalline orientation relationships (the Cu_6Sn_5 has the facet structure, but the β-Sn possesses non-facet structure). In this case, the Cu_6Sn_5 phase has to nucleate more or less homogenously, and no bulk plate-like Cu_6Sn_5 IMCs separates out through the eutectic reaction.

Conclusion

(1) In the explored Sn–Cu alloys, bulk Cu_6Sn_5 IMCs only formed in the slowly cooled Sn–1.0Cu hypereutectic alloy. The strong kinetic undercooling, arising from the rapid solidification condition, leads to actual eutectic point shifting to the direction of higher Cu concentration. Hence, all alloys experienced a metastable pseudoeutectic solidification process.

(2) The volume fraction of bulk Cu_6Sn_5 IMCs in the slowly cooled Sn–1.0Cu alloy could be easily determined from the recorded apparent heat capacity curves. It is larger than the volume fraction of primary Cu_6Sn_5 crystal in the solidified Sn–1.0Cu alloy predicted by the theoretical calculation according to the equilibrium phase diagram. The eutectic Cu_6Sn_5 phase can nucleate around and cling to the primary Cu_6Sn_5 crystal for their matching crystalline orientation relationships, to formed bulk Cu_6Sn_5 IMCs in this alloy.

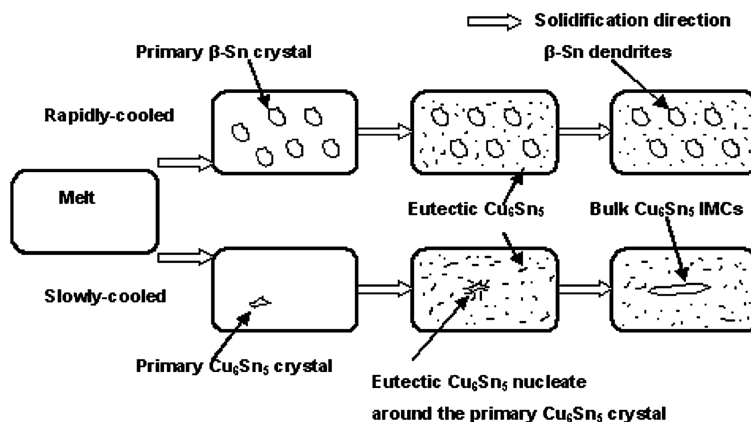

Fig. 8 Schematical diagram exhibiting the separation and growth process of bulk Cu_6Sn_5 IMCs

Acknowledgements The authors are grateful to the National Natural Science Foundation of China (No. 50401003), FANEDD of P R China (No. 200335), and the Natural Science Foundation of Tianjin City (No. 033608811) and Fok Ying Tong Education Foundation (No. 104015) for grant and financial support.

References

1. Abtew M, Selvaduray G (2000) Mater Sci Eng R 27:95
2. Zeng K, Tu KN (2002) Mater Sci Eng R 38:55
3. Laurila T, Vuorinen V, Kivilahti JK (2005) Mater Sci Eng R 49:1
4. Bae KS, Kim SJ (2002) J Mater Res 17:743
5. Suganuma K (2001) Curr Opin Solid State Mater Sci 5:55
6. Lee YG, Duh JG (1998) J Mater Sci 33:5569
7. Lee YG, Duh JG (1999) J Mater Sci: Mater Electron 10:33
8. Islam MN, Chan YC (2005) Mater Sci Eng B 117:246
9. Yoon JW, Kim SW, Jung SB (2004) J Alloys Comp 385:192
10. Yoon JW, Jung SB (2005) J Alloys Comp 396:122
11. Ma X, Wang FJ, Qian YY, Yoshida F (2003) Mater Lett 57:3361
12. Wang FJ , Ma X, Qian YY (2005) Scripta Mater 53:699
13. Kempen ATW, Sommer F, Mittemeijer EJ (2002) Thermo Acta 383:21
14. Moon KW, Boettinger WJ, Kitten UR, Biancaniello FS, Handwerker CA (2000) J Electron Mater 29:1122
15. Chalmers B (1964) Principles of solidification. John Wiley & Sons Inc, New York, p 6
16. Kempen ATW, Sommer F, Mittemeijer EJ, (2002) Acta Mater 50:3545
17. Kim KS, Huh SH, Suganuma K, (2002) Mater Sci Eng A106:333